Chaplygin sleigh in the quadratic potential field

Sergey P. Kuznetsov[1], Vyacheslav P. Kruglov[1,2,3] and Alexey V. Borisov[2]

[1] *Saratov Branch Kotel'nikov Institute of Radioengineering and Electronics of RAS - Saratov, Russia*
[2] *Steklov Mathematical Institute of RAS - Moscow, Russia*
[3] *Yuri Gagarin State Technical University of Saratov - Saratov, Russia*

PACS 5.45.-a – Nonlinear dynamics and chaos
PACS 45.40.-f – Dynamics and kinematics of rigid bodies

Abstract – We study numerically the dynamics of Chaplygin sleigh under action of the quadratic potential field. In contrast with free Chaplygin sleigh our mechanical model manifests complex behaviour: conservative-like chaotic regimes at low energies, coexistent pairs of chaotic attractors and repellers, mapping to each other by time-reversal symmetry, and the recently discovered phenomenon of attractor and repeller intersection, at high energies. We demonstrate that the development of attractors and repellers corresponds to period doubling scenario, followed by their collision and instant increase in size.

Introduction. – Systems with time-reversal symmetry gain attention in nonlinear sciences [1–3] and are especially abundant in mechanics [4–7]. Reversibility is a feature of dynamical system to manifest the same behaviour in forward and backward time evolution. Mathematically speaking, there is a transformation of phase space $\hat{\mathbf{R}}$, called involution, that, when combined with the time-reversal transformation $t \mapsto -t$, leaves the system unchanged. In non-conservative reversible systems the involution maps attractors into repellers and vice versa. An important property of involution is that if it is applied twice, then all of the trajectories are mapped into itself without time reversal: $\hat{\mathbf{R}} \circ \hat{\mathbf{R}} = Id$.

While it is natural to expect Hamiltonian systems to have this property, there are many examples of non-Hamiltonian systems with time-reversal symmetry [8–12]. Among them there are systems with nonholonomic constraints [4–7]. Nonholonomic constraints can not be expressed in terms of coordinates in finite form [13, 14]. Similar to systems with dissipation of energy, the nonholonomic systems lack an invariant measure [15], but often have the energy integral. The well-known example of nonholonomic system is rattleback [4, 16–20] – a semi-ellipsoidal top with one preferred direction of rotation corresponding to attractor, and other direction unstable, corresponding to repeller.

Remarkably, a nonempty intersection of closures of attractor and repeller is possible for some systems with time-reversal symmetry, bringing a new type of dynamics called mixed [21–26], which is distinguished from conservative and pure dissipative. The trajectories of attractors and repellers become intertwined in such a complex manner, that they can not be separated from each other. A particular scenario of mixed dynamics emergence was proposed recently for two-dimensional reversible diffeomorphisms [25, 26]: invariant manifolds of the saddle points belonging to chaotic attractor and to repeller intersect each other, accompanied by collision of the attractor with the repeller. At once the attractor and the repeller instantly increase in size. Such behaviour has been found in the nonholonomic model of the Suslov top and in the dynamics of vortices [25, 26].

The Chaplygin sleigh is the paradigmatic example of nonholonomic system [13, 14]. It is a platform on a plane

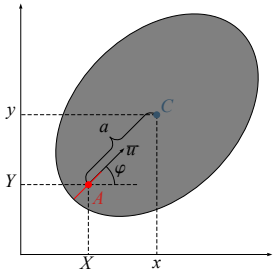

Fig. 1: The Chaplygin sleigh.

surface (fig. 1), supported by two sliding points and a "knife edge", capable of sliding only in the longitudinal direction. One can put a wheel instead of the "knife", with the same constraint. This restriction of translational movement in direction transversal to the "knife edge" is a nonholonomic constraint, which can be physically interpreted as infinite strength of friction [27]. The A marks the contact point of the "knife edge" with the plane and C is the center of mass of the platform, the distance between them is a. The coordinates of A in laboratory frame are X and Y, the coordinates of C are $x = X + a\cos\varphi$, $y = Y + a\sin\varphi$. The longitudinal component of velocity at the point of contact A is $u = \dot{X}\cos\varphi + \dot{Y}\sin\varphi$ and directed along the "knife", the transversal velocity component at the contact point $v = -\dot{X}\sin\varphi + \dot{Y}\cos\varphi$ is zero by constraint. The sleigh is able to rotate around the contact point with angular velocity ω, rotation angle φ is measured between the X axis and the knife.

The dynamics of free Chaplygin sleigh is relatively simple; it is described by an integrable system of equations. Generally, after initial simultaneous translational and rotational movements the sleigh glides in arbitrary direction with constant speed and without rotation. Different modifications of Chaplygin sleigh have been investigated previously: under periodic kicks [28], with additional moving parts, with periodically switched location of nonholonomic constraint [29–33] (with new phenomena of unbounded acceleration [34, 35]), subject to friction [36], and under action of potential forces [37, 38]. Notably, a potential field makes the behaviour much more complicated.

We study the dynamics of Chaplygin sleigh under quadratic potential field, introduced in [38]. The potential force, acting on sleigh, can be applied using the spring under the Hooke's law, that connects the sleigh with the origin point on the plane. In this setup the coordinates play substantial role, but the rotation angle is irrelevant (in rotating reference frame). Conceptually the model of the Chaplygin sleigh moving in potential well resembles the nonlinear oscillator, we even might call our system a nonholonomic oscillator. The motions of the sleigh on the plane are simultaneously oscillatory and rotational, it requires to track four dynamical variables. Therefore, the most suitable way to recognize different dynamical patterns is to visualize typical trajectories in the Poincaré cross-section of the phase space. The phase trajectories are confined by initial conditions to the surfaces of constant mechanical energy, so that we investigate the behaviour of the sleigh at different energy values. Outside the special cases the motions are complex, at different ranges of the energy the dynamics are close to conservative-like or to the typical dissipative-like with period-doubling scenario of chaos onset (with attractors and repellers undergoing simultaneous changes). At very high energies the attractor and repeller visually intersect and parts of them occupy the same space, meaning their trajectories run very close to each other and become practically inseparable [25, 26]. From the practical point of view, this report paves a way to deriving the mathematical model of moving object, capable of complex behaviour without complicated internal machinery, but controllable by external force.

Equations. – One can obtain the model equations with Lagrange–D'Alambert principle. The kinetic energy of the sleigh is:

$$T = \frac{1}{2}\left(mu^2 + (v + a\omega)^2\right) + \frac{1}{2}I\omega^2 = \frac{1}{2}m\left(\dot{X}^2 + \dot{Y}^2 + b^2\dot{\varphi}^2\right) + ma\dot{\varphi}\left(\dot{Y}\cos\varphi - \dot{X}\sin\varphi\right), \tag{1}$$

The last term acknowledges the fact that the center of mass is distanced from the contact point. The components of velocity at contact point in laboratory frame are $\dot{X} = u\cos\varphi$ and $\dot{Y} = u\sin\varphi$, the angular velocity is $\dot{\varphi} = \omega$. Parameter b describes the inertia of the sleigh relative to the contact point: $b^2 = \frac{I}{m} + a^2$.

The constraint is

$$\Gamma = v = -\dot{X}\sin\varphi + \dot{Y}\cos\varphi = 0. \tag{2}$$

The potential energy of the sleigh:

$$U(x, y) = U(X + a\cos\varphi, Y + a\sin\varphi). \tag{3}$$

The equations of motion are given by

$$\frac{\partial T}{\partial q} - \frac{d}{dt}\frac{\partial T}{\partial \dot{q}} - \frac{\partial U}{\partial q} = \lambda\frac{\partial \Gamma}{\partial \dot{q}}, \tag{4}$$

where $q = x$, y or φ, and λ is Lagrange multiplier. After derivations the equations for velocity of the contact point u, angular velocity ω, rotation angle φ and coordinates of the center of mass x and y are

$$\begin{aligned} m\dot{u} &= ma\omega^2 - \frac{\partial U}{\partial x}\cos\varphi - \frac{\partial U}{\partial y}\sin\varphi, \\ mb^2\dot{\omega} &= -ma u\omega + a\frac{\partial U}{\partial x}\sin\varphi - a\frac{\partial U}{\partial y}\cos\varphi, \\ \dot{x} &= u\cos\varphi - a\omega\sin\varphi, \\ \dot{y} &= u\sin\varphi + a\omega\cos\varphi, \\ \dot{\varphi} &= \omega. \end{aligned} \tag{5}$$

Let us specify the potential energy by the function $U = \frac{k}{2}\left(x^2 + y^2\right)$, where k parameter can be interpreted as the stiffness of the spring. With dimensionless variables and parameters

$$\begin{gathered} \tilde{t} = \sqrt{\frac{k}{m}}t, \quad \tilde{u} = \frac{1}{a}\sqrt{\frac{k}{m}}u, \quad \tilde{\omega} = \sqrt{\frac{k}{m}}\omega, \\ \tilde{x} = \frac{x}{a}, \quad \tilde{y} = \frac{y}{a}, \quad \mu = \frac{b^2}{a^2} = \frac{I}{ma^2} + 1, \end{gathered} \tag{6}$$

and omitting the tildes, the equations of motion become

$$\begin{aligned} \dot{u} &= \omega^2 - x\cos\varphi - y\sin\varphi, \\ \mu\dot{\omega} &= -u\omega + x\sin\varphi - y\cos\varphi, \\ \dot{x} &= u\cos\varphi - \omega\sin\varphi, \\ \dot{y} &= u\sin\varphi + \omega\cos\varphi, \\ \dot{\varphi} &= \omega. \end{aligned} \tag{7}$$

After useful change of reference frame

$$\xi = x\cos\varphi + y\sin\varphi, \quad \eta = -x\sin\varphi + y\cos\varphi, \tag{8}$$

the equation for angle φ separates, leaving only four equations:

$$\begin{aligned} \dot{u} &= \omega^2 - \xi, \\ \mu\dot{\omega} &= -u\omega - \eta, \\ \dot{\xi} &= u + \eta\omega, \\ \dot{\eta} &= \omega - \xi\omega. \end{aligned} \tag{9}$$

The dynamics of the angle φ is irrelevant due to the symmetry of the potential and will not be described.

The total mechanical energy of the sleigh is conserved:

$$W = \frac{1}{2}\left(u^2 + \mu\omega^2 + \xi^2 + \eta^2\right). \tag{10}$$

It is important to note, that the divergence of the vector field, associated with eqs. (9), is not zero. Thus, attractors and repellers are possible on the surfaces of constant energy.

There are two involutions:

$$\hat{\mathbf{R}}_1 : \begin{cases} u \mapsto -u, \\ \omega \mapsto -\omega, \end{cases} \quad \text{and} \quad \hat{\mathbf{R}}_2 : \begin{cases} u \mapsto -u, \\ \eta \mapsto -\eta. \end{cases} \tag{11}$$

Their combination is the symmetry:

$$\hat{\mathbf{R}}_1 \circ \hat{\mathbf{R}}_2 = \hat{\mathbf{G}} : \begin{cases} \eta \mapsto -\eta, \\ \omega \mapsto -\omega, \end{cases} \tag{12}$$

which maps trajectories without the time reversal.

The system (9) has a trivial elliptic equilibrium ($u = 0$, $\omega = 0$, $\xi = 0$, $\eta = 0$), corresponding to the center of mass at rest at the bottom of the potential well and the "knife edge" at rest at arbitrary angle φ. If the sleigh does not rotate ($\omega = 0$, $\eta = 0$) while moving, then the center of mass simply oscillates in the potential well like the usual harmonic oscillator:

$$\begin{aligned} \dot{u} &= -\xi, \\ \dot{\xi} &= u. \end{aligned} \tag{13}$$

Our numerical simulations show, that these pure oscillatory motions are unstable with respect to perturbations of ω and η.

If the energy $W > \frac{1}{2}(1+\mu)$, then there are four saddle-focus equilibria ($\xi = 1$, $\omega = \pm 1$, $u \pm \eta = 0$) on the level of energy W. They correspond to revolutions of the sleigh around the bottom of potential well with the center of mass staying at the constant distance $\xi = 1$ counterclockwise ($\omega = 1$, $u = -\eta$) or clockwise ($\omega = -1$, $u = \eta$). The saddle-foci map into each other by involutions $\hat{\mathbf{R}}_1$ and $\hat{\mathbf{R}}_2$ and by the symmetry $\hat{\mathbf{G}}$. At the energy $W = \frac{1}{2}(1+\mu)$ the equilibrium points merge in pairs ($\xi = 1$, $\omega = \pm 1$, $u = 0$, $\eta = 0$) and vanish. At these degenerate equilibria the contact point of the "knife edge" is at the bottom of potential well, while the center of mass rotates around it.

After these trivial considerations, we proceed to discuss the complex dynamics of the Chaplygin sleigh in the quadratic potential. Due to the non-integrability of the eqs. (9), we resort to numerical methods.

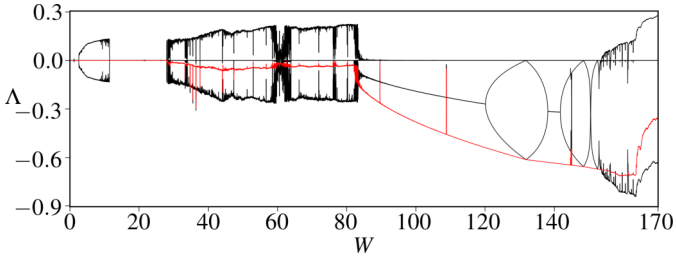

Fig. 2: Lyapunov exponents vs. energy W at $\mu = 10$. Red plot marks the sum of Lyapunov exponents.

Numerical simulations. – Eqs. (9) were solved numerically using the Dormand – Prince method with an adaptive step implemented in the Odeint library from the Boost library collection [39]. The conservation of energy was checked during the simulations.

First, we want to demonstrate what types of behavior are observed in the system by calculating Lyapunov exponents for typical trajectories. The Lyapunov exponents of the trajectory are averaged rates of exponential expansion or contraction of the phase space volume near the trajectory [40]. They characterize the stability of the particular trajectory and are useful tool to identify trajectories of regular or chaotic motions. We used the well-known procedure [41,42] for calculation of Lyapunov exponents with LAPACK subroutines for orthogonalization of perturbation vectors.

Typical dependencies of Lyapunov exponents on energy W are plotted in fig. 2 with energy step $\Delta W \approx 0.00587$. The initial conditions at the adjacent energy steps were picked close to each other to produce more or less continuous plots. We must clarify that for low energies the particular values of Lyapunov exponents differ for every trajectory. Two of the exponents are always zero (up to the numerical accuracy), one is due to the energy integral (the perturbation vectors tangent to the constant energy surface do not grow up or down) and another one corresponds to perturbations along the trajectory, and these have constant average norm. The other two Lyapunov exponents can be nonzero. The positive value of the exponent signifies instability of the trajectory. We plot the sum of Lyapunov exponents with red colour. This sum is the average divergence of the vector field given by right-hand-sides of eqs. (9) along the particular trajectory.

At energies less than $W \approx 28.27$ the sum of Lyapunov exponents is almost equal to zero, therefore the dynamics are close to conservative. One can see, that all values on our plot are zero in the interval of energies from $W \approx 11.43$ to 28.27, because our algorithm accidentally chose initial conditions that belong to trajectories of regular motions, but our numerics show that chaotic trajectories exist in this energy range as well. Our goal for low energies was to show the complexity of possible motions, but our calculations are not representative of the all phase space. We demonstrate below the phase portraits

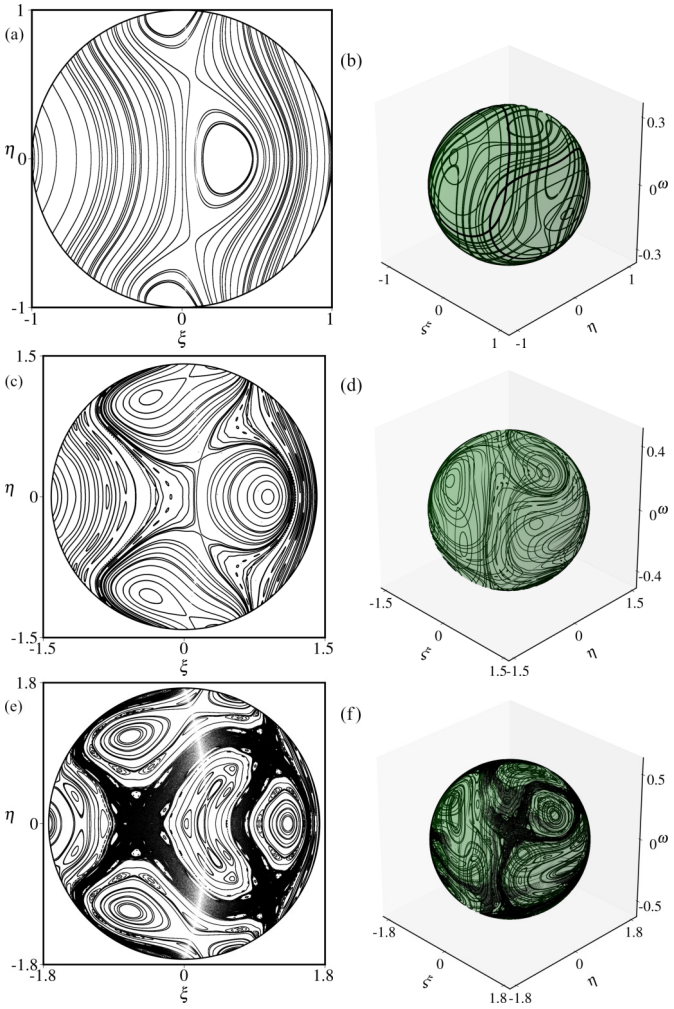

Fig. 3: (a, c, e) Projection of phase space of the Poincaré return map onto the plane of variables ξ and η. Parameter values: $W = 0.5$, 1 and 1.5, while $\mu = 10$. (b, d, f) Portrait of 3D phase space of the Poincaré map. Parameter values: $W = 0.5$, 1 and 1.5, while $\mu = 10$.

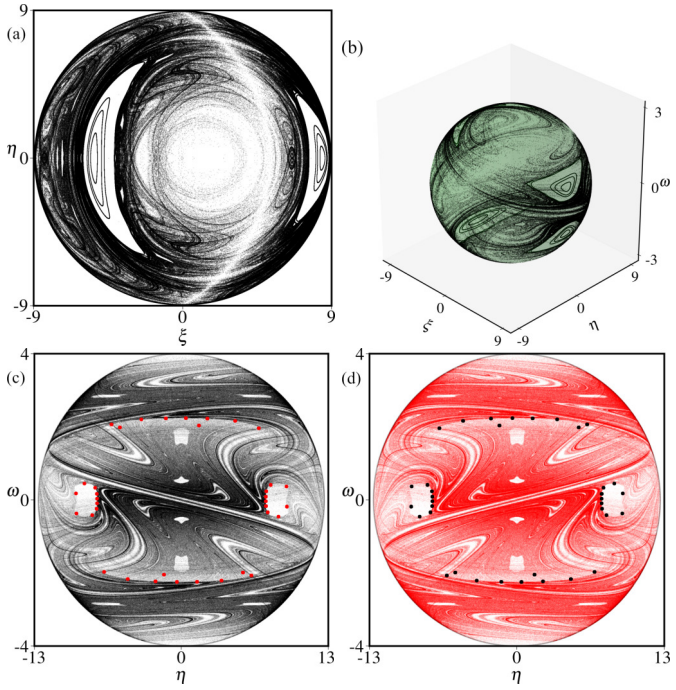

Fig. 4: (a) Projection of phase space of the Poincaré return map onto the plane of variables ξ and η. Parameter values: $W = 40$ and $\mu = 10$. (b) Portrait of 3D phase space of the Poincaré map. Parameter values: $W = 40$ and $\mu = 10$. (c) Phase portrait of forward-time evolution, $W = 80$ and $\mu = 10$. Transients are black, bold red dots mark the limit set after very long simulation – the attractor. (d) Phase portrait of backward-time evolution, $W = 80$ and $\mu = 10$. Transients are red, bold black dots mark the repeller.

of dynamical regimes very similar to conservative, where regular and chaotic trajectories coexist.

At energies more than $W \approx 28.27$ the sum of Lyapunov exponents is slightly less then zero. This is the domain where the attractors, repellers and very intricate transient trajectories coexist. At energies more than $W \approx 80$ the behaviour shifts to clearly dissipative with few attractors and repellers with extremely slow convergence rates. The exact value of energy, where the change of behaviour happens, is unknown to us. For example at $W = 80$ at short times of simulation the dynamics are very complicated, but turns out to be transient, since only simple periodic attractors are observed at sufficiently large times. We should note that there are rare artifacts on the plot at energies $W > 80$ in the form of sharp peaks, which we could not get rid of in the calculations.

At high energies the largest Lyapunov exponent becomes positive with the birth of chaotic attractors. The value of another Lyapunov exponent is zero at some points before the emergence of chaos, indicating bifurcations of regular attractors. At high energies the Lyapunov exponents describe symmetric attractors and repellers with very good accuracy. At $W \approx 163.68$ attracting and repelling domains of phase space overlap with emergence of mixing dynamics. Examples of phase space at these energy values are demonstrated below.

We chose the Poincaré cross-section $u = 0$ (the trajectories cross it in both directions) to portray the dynamics clearly. Due to the energy integral eq. (10) the trajectories of Poincaré return map lie on the ellipsoidal surface $\mu\omega^2 + \xi^2 + \eta^2 = 2W$.

Fig. 3(a) shows the phase portrait of Poincare return map at the energy value $W = 0.5$ projected onto the plane of coordinate variables ξ and η. The phase space is full of quasiperiodic trajectories. Fig. 3(b) shows a three-dimensional phase portrait of the Poincaré map at $W = 0.5$. One can see that the phase space is symmetric to the involutions eqs. (11). Figs. 3(c,d) demonstrate slightly more complicated dynamics at $W = 1$. Figs. 3(e,f) show chaotic layers between quasiperiodic trajectories at $W = 1.5$. We interpret the observed changes in the phase space as the destruction of quasiperiodic trajectories and

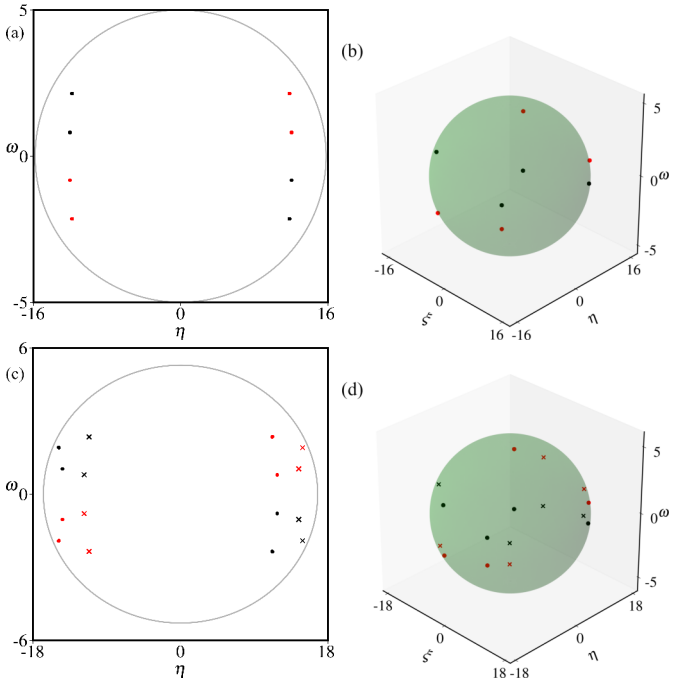

Fig. 5: (a) Attractor and repeller of the Poincaré return map in projection onto the plane of variables η and ω. Parameter values: $W = 125$ and $\mu = 10$. (b) Attractor and repeller in 3D phase space of the Poincaré map. Parameter values: $W = 125$ and $\mu = 10$. Black circles are points of attractor, red circles are points of repeller. (c) Attractors and repellers of the Poincaré return map in projection onto the plane of variables η and ω. Parameter values: $W = 140$ and $\mu = 10$. (d) Attractors and repellers in 3D phase space of the Poincaré map. Parameter values: $W = 140$ and $\mu = 10$. Black circles and crosses are points of two symmetric attractors, red circles and crosses are points of repellers.

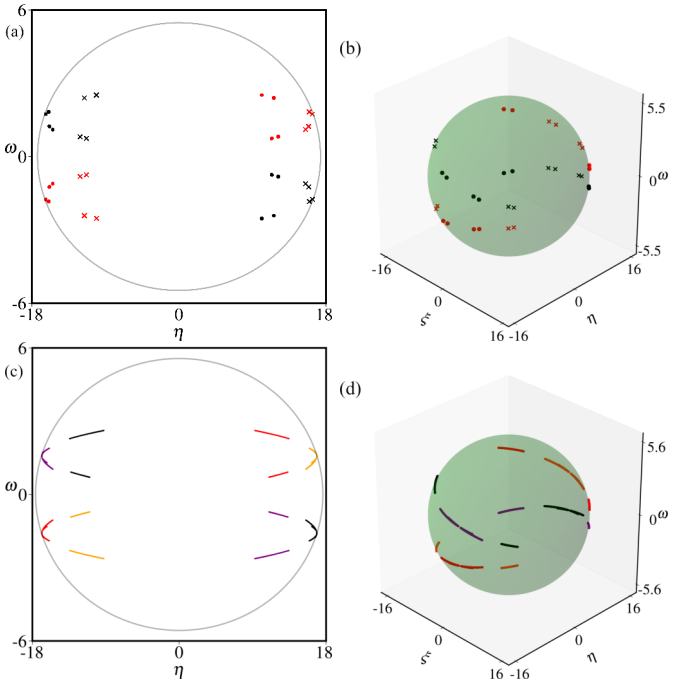

Fig. 6: (a) Attractors and repellers of the Poincaré return map in projection onto the plane of variables η and ω. Parameter values: $W = 150$ and $\mu = 10$. (b) Attractor and repeller in 3D phase space of the Poincaré map. Parameter values: $W = 150$ and $\mu = 10$. Black circles and crosses are points of two symmetric attractors, red circles and crosses are points of repellers. (c) Chaotic attractors and repellers of the Poincaré return map in projection onto the plane of variables η and ω. Parameter values: $W = 155$ and $\mu = 10$. (d) Chaotic attractors and repellers in 3D phase space of the Poincaré map. Parameter values: $W = 155$ and $\mu = 10$. Attractors are plotted black and purple, repellers are plotted red and orange.

formation of chaotic layers. In fact, the KAM-theorem has been proved for general reversible systems without symplectic structure [43–47].

Figs. 4(a,b) show almost complete disappearance of quasiperiodic trajectories at large energies ($W = 40$). Only few quasiperiodic trajectories remain with all Lyapunov exponents equal to zero up to numerical accuracy. But the most of trajectories investigated by us are chaotic with the first Lyapunov exponent positive and the sum of the exponents less than zero. We can not guarantee the existence of chaotic attractors at $W = 40$, since the chaotic trajectories might be very long transients, but we affirm, that after sufficiently long simulations (10^8 iterations of Poincaré return map) the chaotic dynamics endures without changes. At $W = 80$ the dynamics at small times seems to be fully chaotic without quasiperiodic trajectories, but actually at long times (10^8 iterations) all of the trajectories converge to periodic attractor. There is also coexisting periodic repeller, which manifest itself in backward-time simulations. Figs. 4(c,d) show chaotic transients in forward and backward time and periodic attractor and repeller.

At large enough energies the transients become short. Figs. 5(a) and (b) show the attractor and the repeller of Poincaré map at $W = 125$ (recall that the Poincaré cross-section is $u = 0$ in both directions). Both are period-4 cycles and map into each other by involution $\hat{\mathbf{R}}_1$ or $\hat{\mathbf{R}}_2$ or into itself by the symmetry $\hat{\mathbf{G}}$. At $W \approx 131.83$ both the attractor and the repeller undergo pitchfork bifurcations. At figs. 5(c) and (d) one can observe two period-4 regular attractors and two repellers ($W = 140$). Attractors map into repellers by involution $\hat{\mathbf{R}}_1$ or $\hat{\mathbf{R}}_2$, also the attractors map into their symmetric attractors and the repellers map into repellers by the symmetric transformation $\hat{\mathbf{G}}$.

At $W \approx 148.43$ attractors and repellers undergo period doubling bifurcation. Figs. 6(a,b) show two period-8 attractors and two period-8 repellers of Poincaré map at $W = 150$. At the interval of energies [148.53, 153.69] regular periodic attractors and repellers undergo a cascade of period doubling bifurcations, until the chaotic attractors and repellers arise. Examples of pair of chaotic attractors and and pair of repellers are demonstrated at figs. 6(c,d) ($W = 155$).

Approximately at $W \approx 158.5$ two chaotic attractors

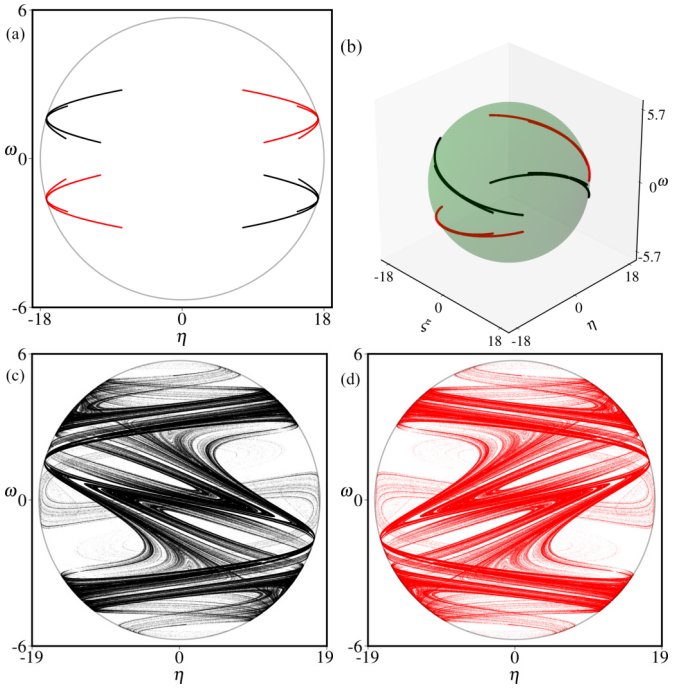

Fig. 7: (a) Chaotic attractor and repeller of the Poincaré return map in projection onto the plane of variables η and ω. Parameter values: $W = 162$ and $\mu = 10$. (b) Attractor and repeller in 3D phase space of the Poincaré map. Parameter values: $W = 162$ and $\mu = 10$. Attractor is plotted black and repeller plotted red. (c) Chaotic attractor of the Poincaré return map in projection onto the plane of variables η and ω. Parameter values: $W = 164$ and $\mu = 10$. (d) Chaotic repeller of the Poincaré return map in projection onto the plane of variables η and ω. Parameter values: $W = 164$ and $\mu = 10$.

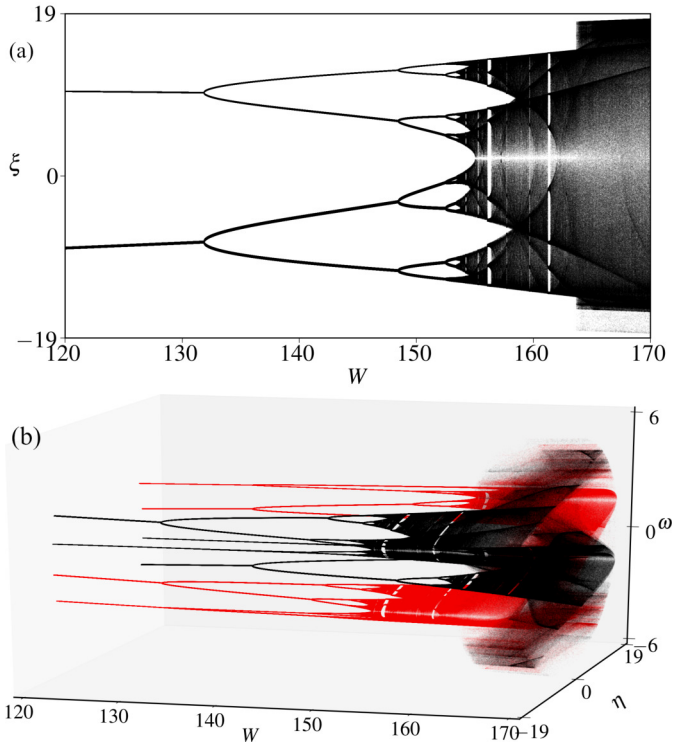

Fig. 8: (a) Bifurcation diagram of attractors (values of ξ vs. energy W). $\mu = 10$. All the attractors are marked black. (b) Bifurcation diagram of attractors and repellers . $\mu = 10$. The slices for particular values of energy W are two-dimensional (variables η and ω). All attractors are marked black, all repellers are marked red.

merge into one and two chaotic repellers merge into one. Figs. 7(a,b) show the only chaotic attractor and the only repeller at $W = 162$. The uncommon phenomenon occurs at $W \approx 163.65$ — the attractor and the repeller merge [25,26]: some of their parts occupy the same regions of phase space. Simultaneously they increase in size explosively. Figs. 7(c,d) demonstrate chaotic attractor and repeller at $W = 164$. One can easily imagine Panels (c) and (d) imposed on each other and see that attractor and repeller are practically inseparable.

Fig. 8(a) demonstrates bifurcation diagram for Poincaré map of (9). Interestingly, a transition to chaos is observed through the Feigenbaum period doubling bifurcation cascade [48]. The estimated convergence constant to the accumulation point corresponds to Feigenbaum's number $\delta = 4.69\ldots$ Such a transition is well known and typical in dissipative nonlinear systems and was also observed in non measure-preserving reversible diffeomorphisms [1,49]. The repellers become chaotic just like the attractors. Fig. 8(b) shows bifurcation diagrams for attractor (black dots) and repeller (red).

Conclusion. – The considered simple model of Chaplygin sleigh under action of the quadratic potential field has a combination of features intrinsic to nonholonomic mechanical systems. It is governed by four-dimensional autonomous system of ordinary differential equations. The system possesses an energy integral and is time-reversible with two distinct involutions, it is not integrable and lacks the invariant measure. The model manifests the destruction of quasiperiodic tori with emergence of chaotic layers at small energies of motion and the period doubling cascade of bifurcations of regular attractors and repellers at high energies, resulting in birth of chaotic attractors and repellers. The chaotic attractors and repellers merge with each other with explosive increase in size. Other nonholonomic systems manifest similar phenomena, but they are more sophisticated in comparison with the example described here. The systems with potential forces are relatively rarely examined in nonholonomic mechanics, so the discussed model is an interesting and missed example. We suppose, that our results may be of interest also to researchers in other areas, where time-reversal symmetry is of substantial role. In the matter of possible practical advantages the investigated mathematical model should be supplemented in future research with modulation of external forces in time as a way of control.

* * *

This work was supported by Russian Science Foundation, grant No. 19-71-30012.

REFERENCES

[1] Roberts J. A. and Quispel G., *Physics Reports*, **216** (1992) 63.

[2] Lamb J. and Roberts J., *Physica D: Nonlinear Phenomena*, **112** (1998) 1.

[3] Lerman L. M. and Turaev D., *Regular and Chaotic Dynamics*, **17** (2012) 318.

[4] Borisov A. V. and Mamaev I. S., *Physics-Uspekhi*, **46** (2003) 393.

[5] Borisov A. V., Mamaev I. S. and Bizyaev I. A., *Regular and Chaotic Dynamics*, **18** (2013) 277.

[6] Borisov A. V., Kazakov A. O. and Sataev I. R., *Regular and Chaotic Dynamics*, **19** (2014) 718.

[7] Bizyaev I. A., Borisov A. V. and Kazakov A. O., *Regular and Chaotic Dynamics*, **20** (2015) 605.

[8] Topaj D. and Pikovsky A., *Physica D: Nonlinear Phenomena*, **170** (2002) 118.

[9] Politi A., Oppo G. and Badii R., *Physical Review A*, **33** (1986) 4055.

[10] Gonchar V. Y., Ostapchuk P., Tur A. and Yanovsky V., *Physics Letters A*, **152** (1991) 287.

[11] Vetchanin E. V. and Kazakov A. O., *International Journal of Bifurcation and Chaos*, **26** (2016) 1650063.

[12] Vetchanin E. V. and Mamaev I. S., *Regular and Chaotic Dynamics*, **22** (2017) 893.

[13] Neimark J. I. and Fufaev N. A., *Dynamics of nonholonomic systems* Vol. 33 (American Mathematical Soc.) 2004.

[14] Bloch A. M., *Nonholonomic mechanics* in *Nonholonomic mechanics and control* (Springer) 2003 pp. 207–276.

[15] Kozlov V., *Uspekhi mekh*, **8** (1985) 85.

[16] Walker G. T., *On a curious dynamical property of celts* in proc. of *Proc. Cambridge Phil. Soc* Vol. 8 1895 pp. 305–306.

[17] Garcia A. and Hubbard M., *Proceedings of the Royal Society of London. A. Mathematical and Physical Sciences*, **418** (1988) 165.

[18] Borisov A. V., Jalnine A. Y., Kuznetsov S. P., Sataev I. R. and Sedova J. V., *Regular and Chaotic Dynamics*, **17** (2012) 512.

[19] Gonchenko A. S., Gonchenko S. V. and Kazakov A. O., *Regular and Chaotic Dynamics*, **18** (2013) 521.

[20] Rauch-Wojciechowski S. and Przybylska M., *Regular and Chaotic Dynamics*, **22** (2017) 368.

[21] Lamb J. S. and Stenkin O. V., *Nonlinearity*, **17** (2004) 1217.

[22] Delshams A., Gonchenko S., Gonchenko V., Lázaro J. and Sten'Kin O., *Nonlinearity*, **26** (2012) 1.

[23] Gonchenko S. V. and Turaev D. V., *Proceedings of the Steklov Institute of Mathematics*, **297** (2017) 116.

[24] Gonchenko A. S., Gonchenko S. V., Kazakov A. O. and Turaev D. V., *Physica D: Nonlinear Phenomena*, **350** (2017) 45.

[25] Kazakov A., *Radiophysics and Quantum Electronics*, **61** (2019) 650.

[26] Kazakov A., *Chaos: An Interdisciplinary Journal of Nonlinear Science*, **30** (2020) 011105.

[27] Fufaev N., *Journal of Applied Mathematics and Mechanics*, **28** (1964) 630.

[28] Borisov A. V. and Kuznetsov S. P., *Regular and Chaotic Dynamics*, **21** (2016) 792.

[29] Bizyaev I. A., Borisov A. V. and Kuznetsov S. P., *EPL (Europhysics Letters)*, **119** (2017) 60008.

[30] Kuznetsov S. P., *EPL (Europhysics Letters)*, **118** (2017) 10007.

[31] Borisov A. V. and Kuznetsov S. P., *Regular and Chaotic Dynamics*, **23** (2018) 803.

[32] Bizyaev I. A., Borisov A. V. and Kuznetsov S. P., *Nonlinear Dynamics*, **95** (2019) 699.

[33] Fedonyuk V. and Tallapragada P., *Nonlinear Dynamics*, **93** (2018) 835.

[34] Bizyaev I. A., Borisov A. V. and Mamaev I. S., *Regular and Chaotic Dynamics*, **22** (2017) 955.

[35] Bizyaev I. A., Borisov A. V., Kozlov V. V. and Mamaev I. S., *Nonlinearity*, **32** (2019) 3209.

[36] Karapetyan A. and Shamin A. Y., *Mechanics of Solids*, **54** (2019) 632.

[37] Borisov A. and Mamayev I., *Journal of Applied Mathematics and Mechanics*, **73** (2009) 156.

[38] Kuznetsov S., *Nonlinear Dynamics*, **15** (2019) 551.

[39] Ahnert K. and Mulansky M., *Odeint – solving ordinary differential equations in c + +* in proc. of *AIP Conference Proceedings* Vol. 1389 (American Institute of Physics) 2011 pp. 1586–1589.

[40] Pikovsky A. and Politi A., *Lyapunov exponents: a tool to explore complex dynamics* (Cambridge University Press) 2016.

[41] Benettin G., Galgani L., Giorgilli A. and Strelcyn J.-M., *Meccanica*, **15** (1980) 9.

[42] Shimada I. and Nagashima T., *Progress of theoretical physics*, **61** (1979) 1605.

[43] Moser J. K. and Webster S. M., *Acta Mathematica*, **150** (1983) 255.

[44] Scheurle J., *Archive for Rational Mechanics and Analysis*, **97** (1987) 103.

[45] Bibikov Y. N. and Pliss V. A., *Differentsial'nye Uravneniya*, **3** (1967) 1864.

[46] Sevryuk M., *Chaos: An Interdisciplinary Journal of Nonlinear Science*, **1** (1991) 160.

[47] Sevryuk M., *Physica D: Nonlinear Phenomena*, **112** (1998) 132.

[48] Feigenbaum M. J., *Journal of statistical physics*, **19** (1978) 25.

[49] Quispel G. and Roberts J., *Physics Letters A*, **135** (1989) 337.